Forschungszentrum Karlsruhe

Technik und Umwelt

Wissenschaftliche Berichte

FZKA 6384

Poloidal MHD flow in the European TAURO blanket concept

L. Bühler

Institut für Kern- und Energietechnik
Projekt Kernfusion

Forschungszentrum Karlsruhe GmbH, Karlsruhe
1999

Poloidal MHD flow in the European TAURO blanket concept

Abstract

The magnetohydrodynamic (MHD) flow of the liquid metal coolant in the plasma facing ducts of the TAURO blanket concept is analyzed. The walls of the channels are fabricated from SiC/SiC composite material which provides good electrical insulation, favorable for a reduction of MHD pressure drop. In the analysis it is assumed that the walls are not perfectly insulating which leads to an electrical coupling of neighboring channels. Results valid for any wall normal conductivity are derived for a model geometry similar to TAURO. The flow structure and pressure drop is evaluated for the designed geometry for both cases, for perfect insulation of the walls and for high wall-normal conductance. It is shown that the increase of pressure drop with the wall conductivity is not really a crucial issue. However, the results show that the flow pattern is strongly affected and may become undesirable for heat transfer when the wall-normal conductivity exceeds a critical value. Proposals are made how the design could be modified for an improved MHD performance.

Poloidale MHD Strömung im Europäischen TAURO Blanket Konzept

Zusammenfassung

In diesem Bericht wird die magnetohydrodynamische (MHD) Strömung in den plasmanahen Kanälen des TAURO Blanket Konzepts untersucht. Die Kanalwände sind aus SiC/SiC hergestellt. Die relativ gute elektrische Isolation dieses Materials ermöglicht eine Reduzierung der MHD Druckverluste. In der Rechnung wird berücksichtigt, daß eine perfekte Isolation nicht möglich ist. Dadurch kommt es zu einer elektrischen Kopplung von benachbarten Kanälen. Für eine TAURO-ähnliche Modellgeometrie werden Ergebnisse hergeleitet, die für beliebige Leitfähigkeit normal zur Kanalwand gelten. Für die im Design vorgesehene Geometrie werden Strömungsverteilungen und Druckverluste berechnet, für den Fall perfekter Isolation sowie für hohe Leitfähigkeiten normal zur Kanalwand. Es wird gezeigt, daß die Zunahme des Druckverlusts als Funktion der Wandleitfähigkeit für die Realisierbarkeit des Konzepts unbedeutend ist. Die Ergebnisse zeigen jedoch einen starken Einfluß der Wandleitfähigkeit auf die Strömungsverteilung, die die Wärmeabfuhr ungünstig beeinträchtigen kann. Abschließend werden Vorschläge gemacht, wie man durch konstruktive Änderungen im Design das MHD Verhalten verbessern könnte.

Contents

1 Introduction

The self-cooled TAURO liquid metal blanket is one of the promising designs for fusion power reactors (Pérez, Giancarli, Molon and Salavy (1995)). The geometry is shown in figure 1 in which the flow paths are indicated. The electrically conducting coolant exerts the strong interactions with the magnetic field confining the fusion plasma. This interaction causes the major part of the pressure drop and determines the flow pattern. The pressure drop is kept on a level as low as possible because the ceramic structural SiC/SiC composite material is almost insulating. Values for the electrical conductivity of the wall material $\sigma_w = 4 \cdot 10^{-5} \frac{1}{\Omega m}$ are given by Pérez et al. (1995), while more recently a value of $\sigma_w = 10^2 - 10^3 \frac{1}{\Omega m}$ for SiC has been reported (M. C. Billone, 1998, included in Tillack, Wang, Pulsifer, Malang, Sze, Billone and Sviatoslavsky (1999)) or values $\sigma_w = 2 - 10^2 \frac{1}{\Omega m}$ are published by a SiC manufacturer (http://www.mortoncvd.com/sicprop1.htm). A value of $\sigma_w = 500 \frac{1}{\Omega m}$ has been used by Giancarli, Bonal, Caso, Marois, Morley and Salavy (1998). All these values are several orders of magnitude lower than that of the fluid at $450^o C$, $\sigma = 7.5 \cdot 10^7 \frac{1}{\Omega m}$ (Malang and Tillack (1995)) and promises small MHD pressure drop. Nevertheless, one should keep in mind that the values reported above hold for unirradiated material, " that the electrical resistivity of SiC varies by at least six orders of magnitude depending on the fabrication technique, impurity content, etc." (personal communication with C. Billone, 1999), and that the degree of irradiation degradation of the electric resistivity is unknown at present day. On the other hand there are indications that a SiC/SiC composite has a conductivity different from that of the pure material. There exists even the possibility that the conductivity of the walls becomes non-isotropic with preferred directions along the enforcing fibers.

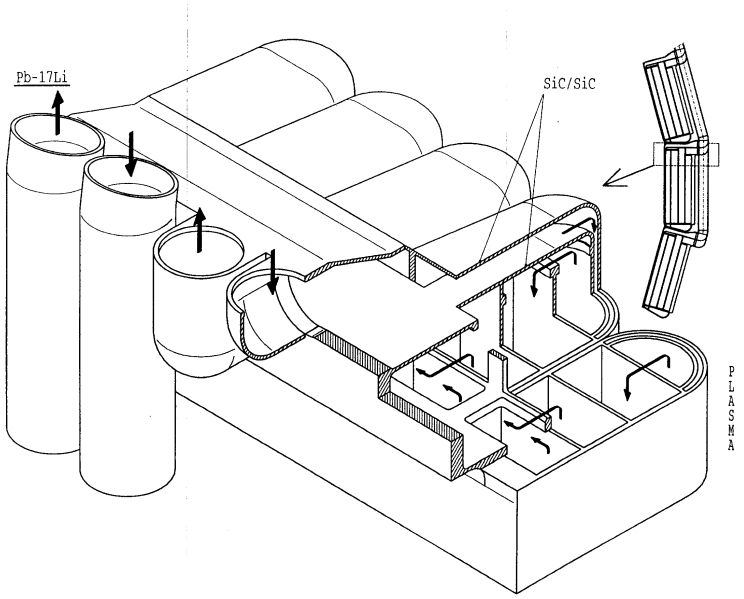

Figure 1: Present design of the TAURO blanket concept, outboard module. 3D rear view, showing the coolant circuit and the collectors. (Pérez et al. (1995))

The geometry of a typical cross section is shown in figure 2. The fluid flows downward through the annular gap ($1.25cm$ in width) with a typical velocity of about $1m/s$. At the bottom of the blanket element the flow changes its direction and returns through the duct 1. The flow passes through several other channels of rectangular cross section along the poloidal direction before it finally leaves the blanket. These channels are not shown here. The flow in these channels is more or less the standard MHD flow as known from a number of references (see .e.g. for a review Moreau (1990) or Hunt (1965), Hunt and Stewartson (1965)).

The MHD flow in the geometry shown in the sketch is considered in more detail since there is little information for the annular gap flow with a transverse magnetic field. There is one reference that considers a similar geometry but uses perfectly or highly conducting walls Kumamaru (1984).He shows results only moderate values of the magnetic field expressed in nondimensional form by the Hartmann number $M = 100$, when the walls have finite but still high conductance. In another reference Miyazaki, Gonno, Nakano, Konishi, Inoue and Yamaoka (1988) consider the flow in a circular tube surrounded by liquid-metal filled gap and find experimentally a pressure drop increase by a factor of 3.6 compared to the case when the annular gap is empty. The walls in the latter publication, however, are electrically conducting so that a comparison with the present application is difficult.

The Hartmann numbers for the TAURO blanket concept are, for the geometry shown in the figure 2, on the order of $M = 2.3 \cdot 10^4$ (based on the dimension of duct 1) using the data for the fluid $Pb - 17Li$ (Malang and Tillack (1995)) at a mean temperature of 450^oC. The conductivity of the walls in tangential direction is poor and may be expressed by the wall conductance ratio $c \approx 1.2 \cdot 10^{-5}$ in non-dimensional form. It can be shown that the currents flowing within the walls in the wall tangential direction are small compared with the currents flowing within the viscous boundary layers. It will be shown in the present work that even for such good insulation properties of the walls there exists a possibility that currents are exchanged between neighboring channels, e.g. between a part of the annular gap, the subregion 2 and the duct 1. This can lead to a strong electromagnetic coupling between both regions and affect the pressure drop and the flow pattern. Flow coupling has been studied e.g. by Molokov (1993). He assumed that the walls are well conducting but since they are very thin their high resistance was responsible for the effects he observed. In his analysis the walls did not offer any resistance against currents passing though the walls from one channel to the other. The rectangular channels were coupled via conducting side walls (parallel to the magnetic field) whereas in the present analysis the channels are coupled though the Hartmann wall, where the magnetic field has a considerable component normal to the wall. This is the reason why the present work and that done by Molokov has almost nothing in common. The present analysis is more closely related to the flow in ducts with insulating coatings reported by Bühler and Molokov (1994), where currents pass normal to the fluid-wall interface through a layer of high resistance. In fact, flow pattern similar to those found in the latter reference will be calculated in the present work.

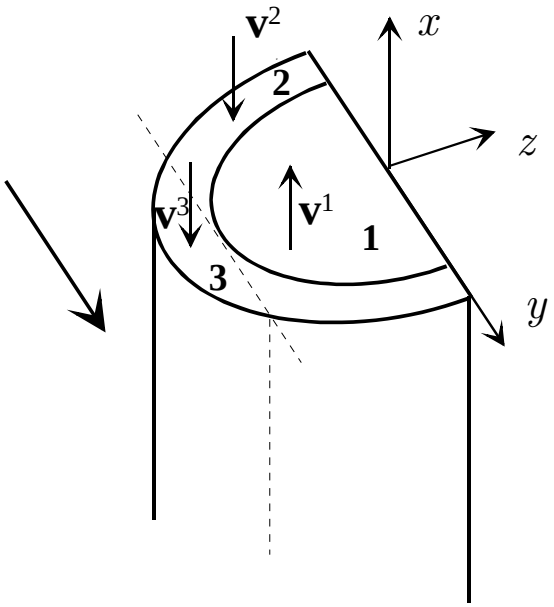

Figure 2: Sketch of the front part of the Tauro blanket concept. The cross sections splits into distinct subregions. One is the central duct 1, where all fluid is returned upward along the x-direction. The other subregions 2 and 3 form an annular gap through which the flow is assumed to have downward orientation. The flow in both parts of the annular gap is separated by a thin viscous layer as indicated by the dashed line. Such layers are generated by singularities at the duct walls and spread along magnetic field lines with typical thickness $\delta_p \sim M^{-1/2}$. Along all curved walls viscous Hartmann layers are present.

2 Formulation

The flow of the electrically conducting coolant in the TAURO liquid metal blanket concept Pérez et al. (1995) is assumed to be fully developed in a typical cross section of the poloidal channels. It is driven by a pressure gradient that may depend on the flow subregion considered. All other flow variables are assumed to be uniform along the flow direction (along the x axis) but may vary within the cross section, here in the yz plane, if the blanket is long enough. For details of the geometry see the sketch in figure 2.

The governing non-dimensional equations reduce by this assumption to the momentum balance along the x-direction

$$M^{-2}\nabla^2 u + K = j_z, \tag{1}$$

and Ohm's law

$$\begin{aligned} j_y &= -\partial_y \phi, & (2)\\ j_z &= -\partial_z \phi + u. & (3) \end{aligned}$$

Conservation of electric charge requires

$$\partial_y j_y + \partial_z j_z = 0. \tag{4}$$

The kinematic boundary conditions are as usual in hydrodynamic flows. At the walls there is no-slip

$$u = 0. \tag{5}$$

It is assumed that the walls are good insulators, say they do not carry a significant amount of current in the tangential direction compared to the current flow within the Hartmann layers. Nevertheless, it is known that the wall material is not a perfect insulator. This is taken into account by the fact that currents may cross the relatively thin walls from one sub-channel to the adjacent one. This condition reads

$$j_n = -s\left(\phi^2 - \phi^1\right) \tag{6}$$

and leads to a strong coupling of the variables in neighboring channels. The superscripts 1 and 2 denote the variables at the fluid wall interfaces in the subregions 1 and 2 respectively. In principle all variables should be characterized by a superscript denoting the corresponding subregions. Unless it is unavoidable these superscripts are omitted for simplicity.

In the equations displayed above u, K, j, and ϕ denote the velocity, the pressure gradient, the current density and potential, scaled by the reference quantities u_0 (average flow velocity, here taken in duct 1, $\sigma u_0 B^2$, $\sigma u_0 B$, and $u_0 a B$, respectively and

$$M = aB\sqrt{\frac{\sigma}{\rho\nu}} \tag{7}$$

is the Hartmann number. A characteristic scale of the duct geometry is a that may be chosen e.g. as the radius of the central duct in TAURO. It is assumed that the fluid is

incompressible with constant density ρ, electrical conductivity σ and kinematic viscosity ν. The parameter

$$s = \frac{\sigma_w a}{\sigma t} \tag{8}$$

denotes the wall-normal conductance ratio of a wall. It becomes obvious that even for small conductivity of the wall, $\sigma_w \ll \sigma$, the parameter s may become large if the wall thickness is small, when $t \ll a$. For the case when a conducting pipe is covered by an electrically insulating layer or coating with thickness t the parameter s corresponds to reciprocal value of the contact or the coating resistance as used e.g. in the analysis of Bühler and Molokov (1993).

One can compare s with the commonly known tangential wall conductance ratio

$$c = \frac{\sigma_w t}{\sigma a}. \tag{9}$$

The relation 6 is valid for $c \ll M^{-1}$, when the Hartmann layers carry much more current along the tangential direction than the wall. A comparison shows that c may be small and s may be large simultaneously for the same conductivity of the wall material so that calculations using the assumptions made above are reasonable.

3 Analysis

For large Hartmann numbers the flow regions split into the inviscid cores surrounded by viscous layers. At walls where the magnetic field has a non-zero normal component the viscous layers are called the Hartmann layers and the corresponding walls are known as the Hartmann walls. The Hartmann layers have typical thickness on the order $\delta \sim M^{-1}$. If an entire wall is parallel to the applied magnetic field the viscous layers are known as the parallel layers or as the side layers. Their thickness is on the order $\delta_p \sim M^{-1/2}$. Layers of similar type appear also between discontinuities at duct walls (tilted rectangular ducts) or as in the present application between the flow regions 2 and 3 (see figure 2). Their role is to match smoothly the solutions in both cores. For thickness of the layers, the flow subregions, and governing equations see e.g. Moreau (1990). The following analysis focuses on the flow in the core and in the Hartmann layers. The flow in the side layers does not carry an order one flow rate if the side wall insulation is high enough (Bühler and Molokov (1993)). Under these conditions the side layers are passive with respect to pressure drop and core velocity and can be excluded from the analysis.

Consider the flow in the core by taking the governing equations in the outer limit as $M \to \infty$. This yields

$$j_{zc} = K, \tag{10}$$

$$j_{zc} = -\partial_z \phi_c + u_c, \tag{11}$$

$$j_{yc} = -\partial_y \phi_c. \tag{12}$$

With conservation of charge one obtains

$$\partial_y j_{yc} = -\partial_{yy} \phi_c = 0. \tag{13}$$

From this equation it becomes obvious that the electric potential in the core depends linearly on y. For y-symmetric problems ϕ_c is constant along field lines.

The inner limit as $M \to \infty$ leads to the equations determining the viscous Hartmann layer contributions as

$$\partial_{\eta\eta} u_\delta - u_\delta = 0 \tag{14}$$

and

$$\phi_\delta = 0. \tag{15}$$

The potential needs no viscous correction across the Hartmann layer and the velocity in the layer is governed by an ordinary differential equation along the stretched coordinate $\eta = M\,(y - Y)$. Here the layer in the flow region 1 at the wall $Y = h\,(z)$ is considered in more detail. Similar layers occur in flow region 2 at the same wall or at the wall $Y = H\,(z)$. The functions $h\,(z)$ and $H\,(z)$ describe the contour of duct 1 and the outer contour of the annular geometry, respectively. It is assumed in the further analysis that the dividing wall at $Y = h$ is relatively thin so that h describes simultaneously the position of the fluid wall interfaces in the duct 1 and in subregion 2 with sufficient accuracy. The general solution that satisfies no-slip at the wall and that vanishes as $\eta \to -\infty$ at large distances from the wall is

$$u_\delta = -u_c \exp\,(\eta) \tag{16}$$

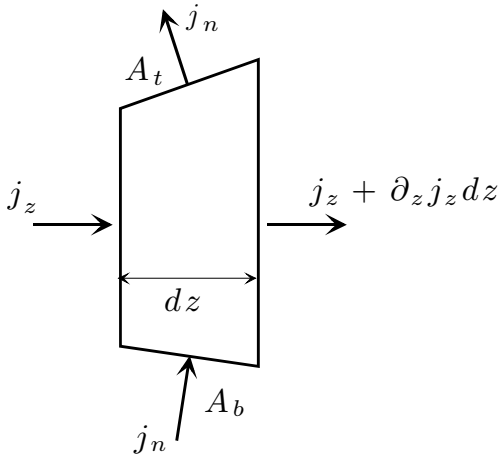

Figure 3: Sketch of the volume element used for the integral formulation of Ohm's law.

and the composite core-Hartmann layer solution becomes

$$u = u_c - u_{ct}\exp(\eta_t) - u_{cb}\exp(\eta_b)\,. \tag{17}$$

This equation takes into account the possibility of two Hartmann layers at the top and at the bottom wall, denoted by the subscripts t and b, respectively. This is the case e.g. in the flow region 2. The velocity u_c may depend on the transverse coordinate z but also on the field aligned coordinate y.

The composite solution for current is obtained from Ohm's law as

$$j_z = K - (K + \partial_z\phi_{ct})\exp(\eta_t) - (K + \partial_z\phi_{cb})\exp(\eta_b)\,. \tag{18}$$

Conservation of charge leads to

$$A_t j_{nt} - A_b j_{nb} + dz\,\partial_z \int_{Y_b}^{Y_t} j_z dy = 0, \tag{19}$$

when applied in an integral sense. For details of the geometry see figure 3. Here, $A_t = \sqrt{1+Y_t'^2}dz$ and $A_b = \sqrt{1+Y_b'^2}dz$ are the areas at the top and bottom of a volume element with width dz and the corresponding Y' denote differentiation with respect to z. The equation (19) finally gives

$$\sqrt{1+Y_t'^2}j_{nt} - \sqrt{1+Y_b'^2}j_{nb} + K\,(Y_t' - Y_b') - M^{-1}\partial_{zz}\,(\phi_{ct} + \phi_{cb}) = 0. \tag{20}$$

This equation accounts for the global balance of charge within a volume element that extends along field lines from one wall to the other.

By similar reasoning one can extract an analog relation that accounts for a charge balance in a volume element which is bounded in y-direction at one side by a wall and by the core at the other side. This yields at the bottom wall

$$j_{yc} - \sqrt{1+Y_b'^2}j_{nb} - KY_b' - M^{-1}\partial_{zz}\phi_{cb} = 0 \tag{21}$$

and at the top wall

$$\sqrt{1+Y_t'^2}j_{nt} - j_{yc} + KY_t' - M^{-1}\partial_{zz}\phi_{ct} = 0. \tag{22}$$

The summation of the last two equations is recovered in equation (20). For abbreviations in the following and overbar is used to denote values averaged along y such as $\bar{\phi}_c = (\phi_{ct} + \phi_{cb})/2$ and the half difference between values at the top and bottom is indicated as $\Delta\phi_c = (\phi_{ct} - \phi_{cb})/2$. Then equation (20) becomes

$$\frac{1}{2}\left(\sqrt{1+Y_t'^2}j_{nt} - \sqrt{1+Y_b'^2}j_{nb}\right) + K\Delta Y' - M^{-1}\partial_{zz}\bar{\phi}_c = 0. \tag{23}$$

The difference of equations (22) and (21) results in

$$\frac{1}{2}\left(\sqrt{1+Y_t'^2}j_{nt} + \sqrt{1+Y_b'^2}j_{nb}\right) + \frac{\Delta\phi_c}{\Delta Y} + K\bar{Y}' - M^{-1}\partial_{zz}\Delta\phi_c = 0, \tag{24}$$

when the uniform potential gradient is expressed as $j_{yc} = -\frac{\phi_{ct}-\phi_{cb}}{Y_t-Y_b}$. This is an equation which governs the potential difference between the top and the bottom wall of a duct.

This leads within the subregions 1, 2 and 3 to the following equations relating the core potentials as

$$\sqrt{1+h'^2}s\left(\bar{\phi}_c^1 - \bar{\phi}_c^2 + \Delta\phi_c^2\right) + K^1h' - M^{-1}\partial_{zz}\bar{\phi}_c^1 = 0, \tag{25}$$

$$-\sqrt{1+h'^2}s\left(\bar{\phi}_c^1 - \bar{\phi}_c^2 + \Delta\phi_c^2\right) + K^2\left(H'-h'\right) - 2M^{-1}\partial_{zz}\bar{\phi}_c^2 = 0, \tag{26}$$

$$\sqrt{1+h'^2}s\left(\bar{\phi}_c^1 - \bar{\phi}_c^2 + \Delta\phi_c^2\right) + 4\frac{\Delta\phi_c^2}{H-h} + K^2\left(H'+h'\right) - 2M^{-1}\partial_{zz}\Delta\phi_c^2 = 0 \tag{27}$$

$$K^3H' - M^{-1}\partial_{zz}\bar{\phi}_c^3 = 0. \tag{28}$$

These equations are derived with the assumption of y-symmetry in the subregions 1 and 3, say $j_n = j_y = 0$ at $y = 0$. The potential differences $\Delta\phi_c^2$ and $\Delta\phi_c^3$ vanish due to symmetry in these subregions. At the symmetry plane there is no Hartmann layer. This is the reason why the M^{-1} term appears only once in these sub-regions, while it appears twice in subregion 2 where two Hartmann layers are present. It is further assumed that the wall at $y = H$ is insulating, i.e. $j_n = 0$ and that the pressure drops in subregions 2 and 3 are equal, $K^3 = K^2$, since both are hydraulically connected.

The main task to be solved is the solution of the last four equations for the potentials. Once the potentials are determined it is possible to reconstruct the velocity profiles according to Ohm's law (11) and to calculate the flow rates in the subregions.

4 Results for a model geometry

General solutions to the equations derived above are possible only numerically. To get insight into the physical behavior of the flow the geometry is simplified as shown in the sketch in figure 4. The central channel is approximated by a rectangle, the annular gap by rectangular regions. Of course, such a change in geometry will change the flow quantities. Nevertheless the main features are preserved. It should therefore be possible to draw the main conclusions from the simplified model, which allows to cover a large range of the wall-normal conductance parameter s ranging from insulating conditions to high conductance.

In other sections the attention will be focused on a more relevant geometry. For that case it will be possible to derive solutions for perfect insulation of the walls and solutions for the case of high wall-normal conductance.

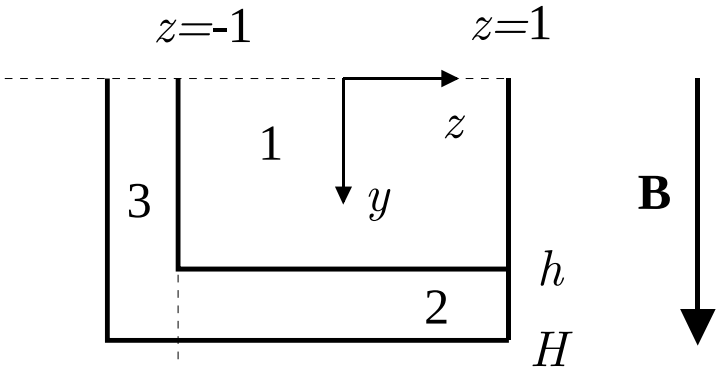

Figure 4: Simplified geometry used as a model to explain the MHD phenomena expected in the Tauro blanket concept.

For the model geometry the functions h and H do not depend on z, i.e. $h' = H' = 0$. The equations determining the potentials then become

$$\frac{2}{3}\mathsf{s}^2\left(\bar{\phi}_c^1 - \bar{\phi}_c^2\right) - \partial_{zz}\bar{\phi}_c^1 = 0, \tag{29}$$

$$-\frac{2}{3}\mathsf{s}^2\left(\bar{\phi}_c^1 - \bar{\phi}_c^2\right) - 2\partial_{zz}\bar{\phi}_c^2 = 0, \tag{30}$$

$$\partial_{zz}\bar{\phi}_c^3 = 0, \tag{31}$$

independent of the pressure drops K^1 and K^2. The variable s has been replaced as $sM = \frac{2}{3}\mathsf{s}^2$ in order to get a simpler representation of the results.

In these equation the potential difference $\Delta\phi_c^2$ of subregion 2 is no longer present. The reason for neglecting $\Delta\phi_c^2$ is outlined briefly. It has been assumed at the beginning that the walls are poor conductors, $s \ll 1$. This allows to omit the wall normal currents from the equation (27) in comparison with the current j_{cy} (the second term). The remaining terms are

$$2\frac{\Delta\phi_c^2}{H-h} - M^{-1}\partial_{zz}\Delta\phi_c^2 = 0. \tag{32}$$

Order of magnitude arguments suggest that $\Delta\phi_c^2$ has boundary layers of thickness $\delta \sim O\left(\left(\frac{H-h}{M}\right)^{1/2}\right)$. These layers are even thinner than the viscous side layers which are not treated by the present analysis. If $\Delta\phi_c^2$ reaches magnitudes on the order of one or smaller within these layers, $\Delta\phi_c^2$ is exponentially small everywhere else in the domain under consideration.

The solutions are obtained as

$$\begin{aligned}
\partial_z\phi_c^1 &= A - 2B\cosh(\mathsf{s}z) - 2C\sinh(\mathsf{s}z), && (33)\\
\partial_z\bar{\phi}_c^2 &= A - B\cosh(\mathsf{s}z) - C\sinh(\mathsf{s}z), && (34)\\
\partial_z\phi_c^3 &= D. && (35)
\end{aligned}$$

The unknown constants of integration $A-C$ are determined by the fact that at the left and right side of the subregion 1 and at the right side of subregion 2 the integral current must vanish when the side walls are assumed to be insulating.

$$\begin{aligned}
\textstyle\int_0^h j_z^1 dy &= K^1 h - M^{-1}\partial_z\bar{\phi}_c^1 &&= 0, \quad \text{at} \quad z=-1;\\
\textstyle\int_0^h j_z^1 dy &= K^1 h - M^{-1}\partial_z\bar{\phi}_c^1 &&= 0, \quad \text{at} \quad z=1; \qquad (36)\\
\textstyle\int_h^H j_z^2 dy &= K^2(H-h) - 2M^{-1}\partial_z\bar{\phi}_c^2 &&= 0. \quad \text{at} \quad z=1.
\end{aligned}$$

These conditions are equivalent to those used in Bühler and Molokov (1994). The currents induced in the core enter the side layer. In the side layer they turn towards the Hartmann layers. They enter the Hartmann layers before they can be exchanged between the subregions. The unknown D is obtained by the fact that all current induced in the core of subregion 3 must return through the Hartmann layer.

$$\textstyle\int_0^H j_z^3 dy = K^2 H - M^{-1}\partial_z\bar{\phi}_c^3 = 0, \qquad (37)$$

The key point of the overall analysis is that the side walls are insulators and that the side layers have a passive role in the sense that they distribute the currents from the core to the corresponding Hartmann layers with negligible resistance. The results after applying these boundary conditions become

$$\begin{aligned}
A &= \frac{1}{3}M\left[K^1 h + K^2(H-h)\right], && (38)\\
B &= \frac{1}{3}M\left[-K^1 h + \frac{1}{2}K^2(H-h)\right]\frac{1}{\cosh(\mathsf{s})}, && (39)\\
C &= 0, && (40)\\
D &= MK^2 H. && (41)
\end{aligned}$$

In a further step one can combine the equation (17) determining the velocity with Ohm's law (11) and find

$$\bar{u} = \partial_z\bar{\phi} \qquad (42)$$

at the leading order of approximation for each subregion. The corresponding flow rates are obtained by integration over the sub-regions.

$$q^1 = h\int_{-1}^{1} \bar{u}^1 dz, \tag{43}$$

$$q^2 = (H-h)\int_{-1}^{1} \bar{u}^2 dz, \tag{44}$$

$$q^3 = H\int_{-1-b}^{-1} \bar{u}^3 dz. \tag{45}$$

Here, b is the width of the gap in subregion 3. It will be later used equal to the gap size in subregion 2.

All flow has to pass through subregion 1. This flow rate is fixed by definition to

$$q^1 = 2h, \tag{46}$$

which is equivalent with choosing the velocity scale u_0 as the average velocity in duct 1. The equation (46) and the condition on the integral flow rate

$$q^1 + q^2 + q^3 = 0 \tag{47}$$

determines finally the pressure drops K^1 and K^2.

Results are compared with those of perfect insulation, say the pressure drops are normalized with that in region 1 if there were no currents passing through the walls ($s = 0$), the pressure drops decuple and

$$K^1_{ins} = (Mh)^{-1}. \tag{48}$$

It is shown in figure 5 that the pressure drop in sub-channel 1 keeps the order of magnitude even is the walls are highly conducting in the wall-normal direction. Depending on the parameters used the pressure drop can become larger by a factor of roughly 5 as $sM \to \infty$ compared with the case of perfect insulation. The geometry parameter $\alpha = H/h$ has been introduced to study the influence of changes in the geometry.

The pressure drop in the regions 2 and 3 may become even larger. This has its reason mainly by the fact that the subregions 2 and 3 have relatively narrow cross sections requiring high velocities and thus giving rise to high pressure drops. The increase of pressure drop with the wall normal conductivity is not so significant.

More interesting, however, are the flow rates carried by the distinct subregions. For $sM \to 0$ there exists a downflow in subregion 2 and upflow in duct 1. This corresponds to the intension of the TAURO designers, where in regions 2 and 3 the flow direction is opposite to that in duct 1. The flow carries by region 2 is relatively small, $7.5 - 15\%$ for α between 1.1 and 1.3. The remaining part of the flow is carried by subregion 3. This may be favorable concerning heat transfer, because the heat input to subregion 3 is highest. However, if the wall normal conductivity reaches a certain value the flow direction in region 2 turns. For larger values of the product sM the flow will become reversed compared with the envisaged (designed) velocity. The flow in this sub-region becomes increasingly coupled by electric currents to the flow in duct 1. Since the net

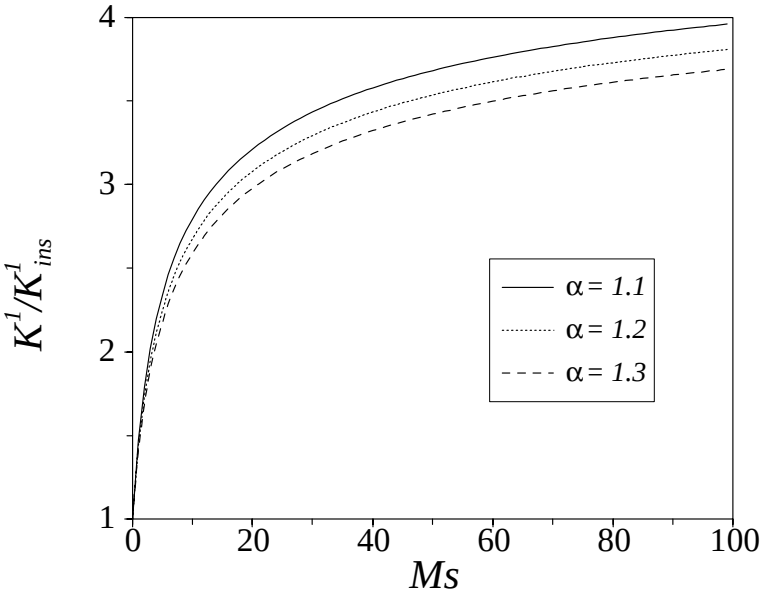

Figure 5: Pressure drop in duct 1 as a function of the product Ms. For $Ms \to 0$ the pressure drop approaches values as in insulating channels. For $Ms \to \infty$ the pressure drop is higher than in insulating channels by a finite factor depending on the geometry.

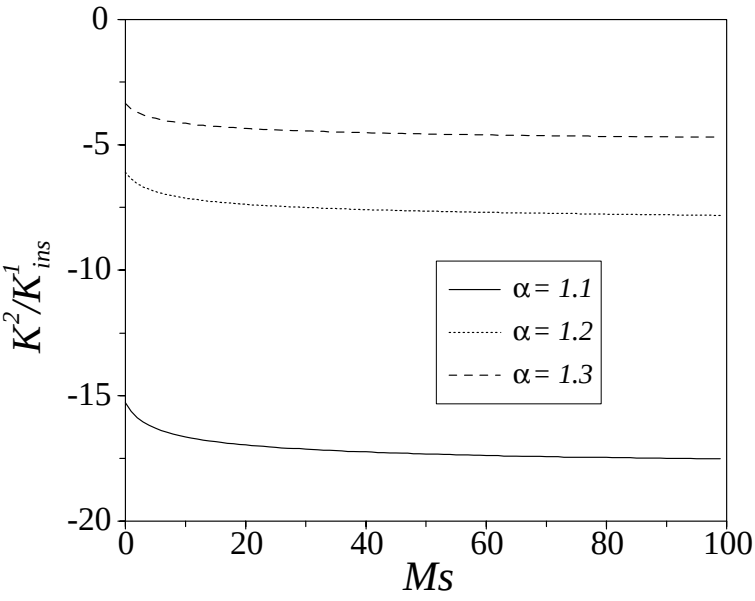

Figure 6: Pressure drop in subregions 2 and 3 as a function of the product Ms.

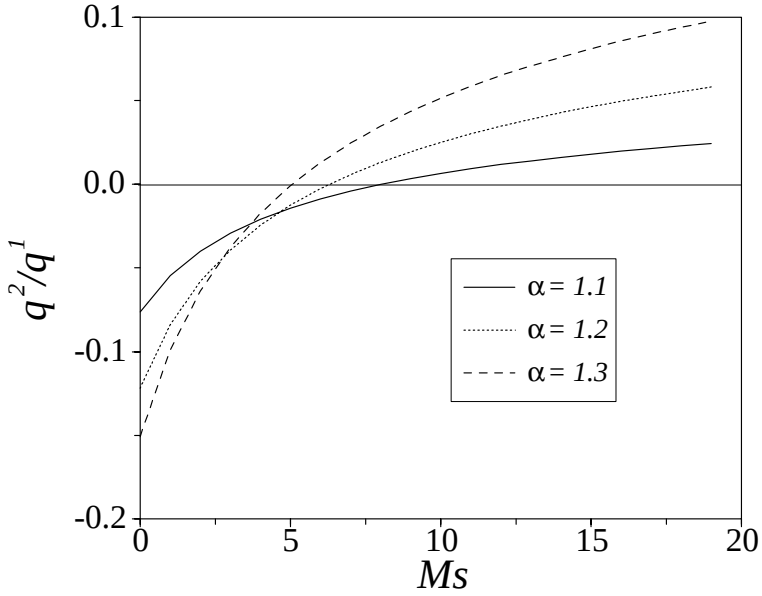

Figure 7: Ratio of flow rates between subregion 2 and duct 1. For small values of the wall normal conductivity, $Ms \to 0$ the direction of the flow is as foreseen by the design. There is downflow in subregion 2 and upflow in duct 1. For larger values of Ms there exists a possibility that the flow in subregion 2 becomes reversed. The value of Ms for which this will happen depends on the geometry parameter α.

flux in regions 2 and 3 has to balance the flux in duct 1 the region 3 has to carry a much larger amount. This increases the velocities in this region and the pressure drop.

The flow reversal in the region 2 may have severe consequences concerning heat transfer. This has its reason in the fact that stationary recirculation cells will appear circulating fluid in the poloidal direction, upward in regions 2 and downward in region 3. This will inhibit heat exchange from region 2 and from a part of region 3.

Of course, the model has been simplified greatly by changing the geometry. Calculations performed during the next section using the more relevant geometry will show different numbers but the tendency and the order of magnitude of the phenomena observed will be consistent with the results outlined just above. One can conclude further, that the severe implications do not occur if the wall is well insulating in the direction normal to the wall. This means that the quantity s or the product sM should be very small,

$$\mathsf{s} \text{ or } sM \ll 1. \tag{49}$$

This is a much stronger demand on the insulation properties of the wall material than the condition that no significant currents should flow inside the wall in the tangential direction where the condition

$$Mc \ll 1 \tag{50}$$

was sufficient to ensure a behavior as in ducts with insulating walls. The new relation requires insulating properties in terms of wall conductivity that are by a factor $\left(\frac{t}{a}\right)^2$ smaller than those required previously.

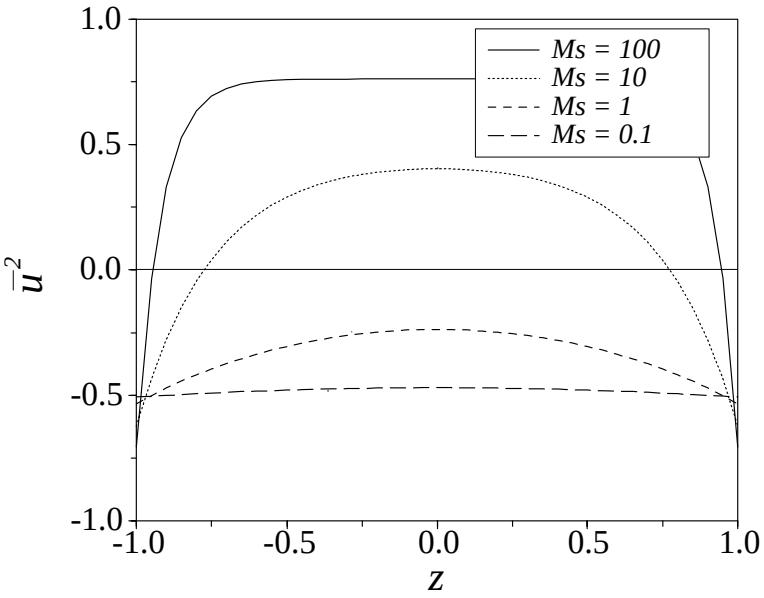

Figure 8: Velocity profile $u^2(z)$ in subregion 2 for an aspect ratio $\alpha = H/h = 1.3$ for different insulating qualities Ms.

Finally the core velocity profile in the duct 2 is discussed in some detail. Results are shown in figure 8 as a function of the z-position in the cross section. If the separating wall at $y = h$ is highly insulating, $sM = 0.1$ the flow in the whole subregion is downward. If the insulation is worse, the flow exhibits a profile along z with exponential layers near $z = \pm 1$. The thickness of these layers is on the order s^{-1} or in original quantities on the scale $(sM)^{-1/2}$. The flow becomes reversed first in the center of the subregion 2. The result is that there will exist two closed loops of flow. One is near $z = 1$, where the downward flow is compensated by a part of the upward flow at larger distance from the wall. The other loop will be generated by the remaining upward flux which is balanced by downward flow in the same subregion near $z = -1$ and by an increased downward flow in region 3.

Similar results exist if the flow in duct 1 is considered. Results are shown in figure 9. The velocity profile is uniform along z if the walls are well insulating. On the other hand the flow develops boundary layers as discussed already if the quantity sM becomes large. Nevertheless, the flow in duct 1 will never be reversed, a fact that may be positive when heat transfer by volumetric heating is to be considered. For strong coupling the velocities in both, the duct 1 and subregion 2 become equal except within the exponential layers.

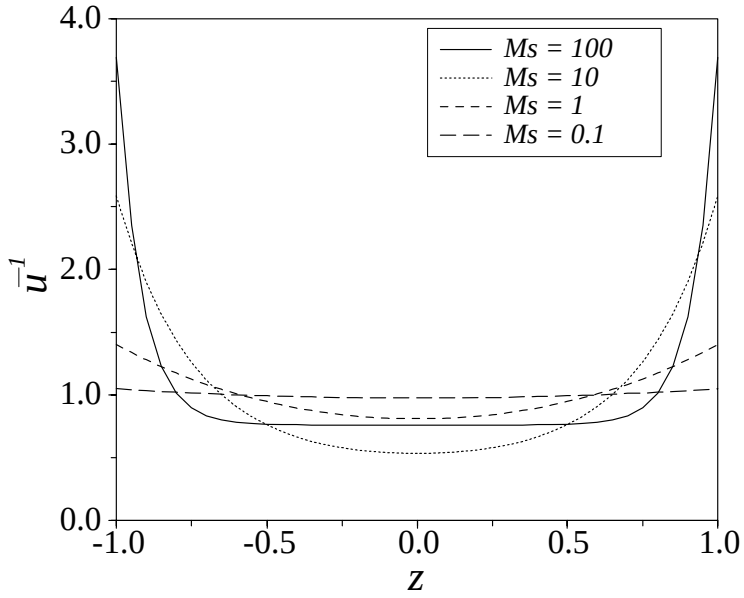

Figure 9: Velocity profile $u^1(z)$ in duct 1 for an aspect ratio $\alpha = H/h = 1.3$ for different insulating qualities Ms.

5 Results for TAURO

In this section the attention is redrawn to the original geometry of TAURO. Unlike in the previous section it is not possible to cover the whole range of the parameter s, but the case of high wall-normal conductance $sM \gg 1$ and the desirable case of insulating walls $sM \ll 1$ can be solved by using similar methods as outlined just above for the model geometry. For sM near unity the governing equations become intractable by analytical techniques. A solution in this range of values should be performed preferentially by numerical methods if it turns out that it is required for TAURO.

5.1 Perfectly insulating walls

In a first step the flow in the TAURO geometry (see figure 2) is considered assuming perfect insulation of the duct walls. Perfect insulation requires $s = 0$ (as well as $c = 0$) and the equations determining the potentials in the distinct subregions decuple. An integration of the equations (25-28) leads to the potential gradients

$$\partial_z \bar{\phi}_c^1 = MK^1 h, \tag{51}$$

$$\partial_z \bar{\phi}_c^2 = \frac{1}{2} MK^2 \left(H - h\right), \tag{52}$$

$$\partial_z \bar{\phi}_c^3 = MK^2 H. \tag{53}$$

The integration constants evaluate to zero because the integral current balance (the composite solution, equation 18) requires in insulating ducts

$$\int_{Y_b}^{Y_t} j_z dy = 0. \tag{54}$$

This means physically that all current induced in the core has to return via the corresponding Hartmann layers. From the results for potential gradient one can evaluate the velocity according to Ohm's law up to the leading order as $\bar{u}_c = \partial_z \bar{\phi}_c$ and obtain for the different subregions

$$\bar{u}_c^1 = MK^1 h, \tag{55}$$

$$\bar{u}_c^2 = MK^2 \left(H - h\right)/2, \tag{56}$$

$$\bar{u}_c^3 = MK^2 H. \tag{57}$$

These results are typically for MHD flows in insulating ducts, where the profile of velocity $\bar{u}\left(z\right)$ always take values proportional to the dimension of the cross section measured along magnetic field lines, here e.g. $\bar{u}_c^1 \sim h\left(z\right)$, in accordance with Chang and Lundgren (1961). Note, the quantity $\Delta\phi_c^2$ does not enter the solution for average velocity and is therefore unimportant for the determination of the pressure drop.

The solution in duct 1 can be obtained independently from those in the other subregions. If the flow rate in this duct

$$q^1 = \int_{-1}^{0} \bar{u}_c^1 h \, dz = \frac{1}{4}\pi \tag{58}$$

is fixed such that the average velocity becomes unity, one obtains the well known solution for the pressure drop in insulating pipes (Gold (1962))

$$K^1 = \frac{3\pi}{8M}, \tag{59}$$

using a circular shape of the duct as $h = \sqrt{1-z^2}$.

The flow rate in subregion 3 is evaluated similarly as

$$q^3 = \int_{-\alpha}^{-1} u_c^3 H dz = \frac{1}{3}\left(2\alpha - 1\right)\left(\alpha - 1\right)^2 MK^2 \tag{60}$$

by assuming the outer contour $H = \sqrt{\alpha^2 - z^2}$. Here, α is the aspect ratio of the outer to the inner wall radius. This result is plausible considering the fact that at a fixed pressure gradient the flow rate vanishes as $\alpha \to 1$, when the gap becomes infinitesimally small.

Analog considerations lead to the flow rate in subregion 2

$$\begin{aligned} q^2 &= \int_{-1}^{0} \bar{u}_c^2 \left(H - h\right) dz, \\ &= \frac{1}{3}\left[\frac{1}{2}\left(3\alpha^2 + 1\right) + \alpha\left(\alpha^2 - 1\right)\mathrm{K}\left(\frac{1}{\alpha}\right) - \alpha\left(\alpha^2 + 1\right)\mathrm{E}\left(\frac{1}{\alpha}\right)\right] MK^2, \end{aligned} \tag{61}$$

where $\mathrm{K}\left(\frac{1}{\alpha}\right)$ and $\mathrm{E}\left(\frac{1}{\alpha}\right)$ are the complete elliptic integrals of first and second kind. When α is near unity one can derive a simplified version, valid for small annular gap sizes. Then the relation

$$q^2 \approx \frac{1}{6}\left[\frac{5}{4} + \frac{3}{2}\ln\left(\alpha - 1\right) - 3\ln\left(2\sqrt{2}\right)\right]\left(\alpha - 1\right)^2 MK^2 \quad \text{for } \alpha \to 1 \tag{62}$$

approximates the flow rate.

Finally, all fluid that flows down through the annular gap formed by the subregions 2 and 3 must return through duct 1. This leads to the integral flow balance

$$q^1 + q^2 + q^3 = 0, \tag{63}$$

which is used to determine the pressure drop K^2.

In figure 10 the flow rates in subregions 2 and 3 are plotted. They are normalized with the flow rate in duct 1 so that their sum will give always a value of $q^2/q^1 + q^3/q^1 = -1$. It can be seen that for $\alpha \to 1$ the flow rate in region 3 vanishes and all flow is carried by the region 2. The reason for such a behavior is that the area of cross section for subregion 3 decreases more rapidly than the velocity in this domain is increased when α approaches unity. On the other hand, when $\alpha \to \infty$, the area of subregion 3 increases more rapidly than that in subregion 2 with the result that all flow is carried by region 3. The latter case with $\alpha \gg 1$, however, is not interesting for the applications envisaged.

One of the key results for the Tauro blanket concept is the total pressure drop

$$K_{tot} = K^1 + \left|K^2\right| \tag{64}$$

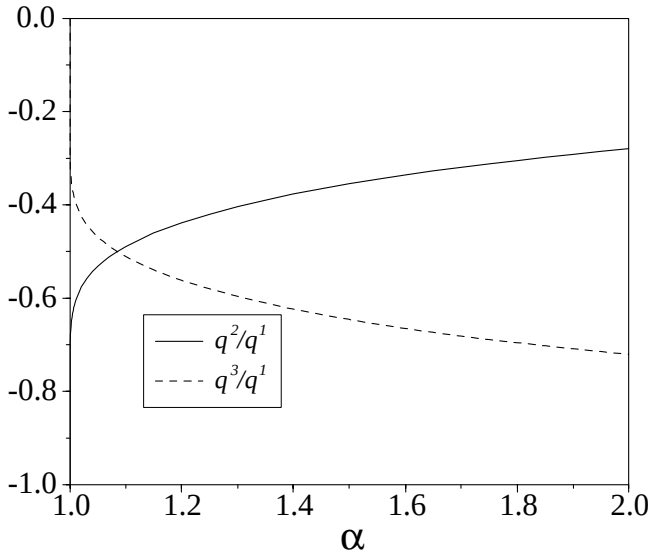

Figure 10: Flow rates in subregions 2 and 3, normalized with flow rate in duct 1. For $\alpha \to 1$ all flow is carried within subregion 2.

that the fluid exerts when passing downward and upward through a blanket section of one characteristic length. This quantity can be normalized with the pressure drop in duct 1 and evaluated as

$$\frac{K_{tot}}{K^1} = 1 + 2\left[\alpha\left(\alpha^2-1\right)\mathrm{K}\left(\frac{1}{\alpha}\right) - \alpha\left(\alpha^2+1\right)\mathrm{E}\left(\frac{1}{\alpha}\right) - \frac{3}{2}\left(\alpha^2-1\right) + 2\alpha^3\right]^{-1} \qquad (65)$$

and is plotted in figure 11 as a function of the aspect ratio α. The pressure drop increases strongly as $\alpha \to 1$ but approaches the value as in the insulating circular pipe in duct 1 as $\alpha \gg 1$. The evaluation of the pressure gradient K_{tot} of the flow in the gap and in duct 1 for the present TAURO geometry yields $K_{tot} = 0.0053 MPa/m$, a value that is negligible in comparison with the hydrostatic pressure head. In addition the average velocities U^2 and U^3 in the regions 2 and 3 are shown in the same figure. For small values of α the average velocity in subregion 3 increases more rapidly than the average velocity in subregion 2. This may be favorable for heat transfer in the present application since the heat flux entering the region 3 is higher than the one in region 2. Nevertheless one should notice, that the pressure drop increases faster than any average velocity. Benefits in heat transfer may be smaller than the disadvantages from increasing pressure drop and one should carefully choose the optimum value of α. For the present TAURO the MHD pressure drop is very small so that an increase in velocity seems reasonable if required for heat transfer.

Core velocity profiles are plotted in figure 12 as a function of the z coordinate. As aspect ratio a value of $\alpha = 1.3$ has been chosen. The velocity in subregion 3 behaves as expected for insulating pipe flow, i.e. the velocity increases proportional to the channel height measured along magnetic field lines, $\bar{u}_c^3 \sim H$, and reaches its maximum absolute value at $z = -1$. Passing from subregions 3 to 2 the core velocity drops to half the

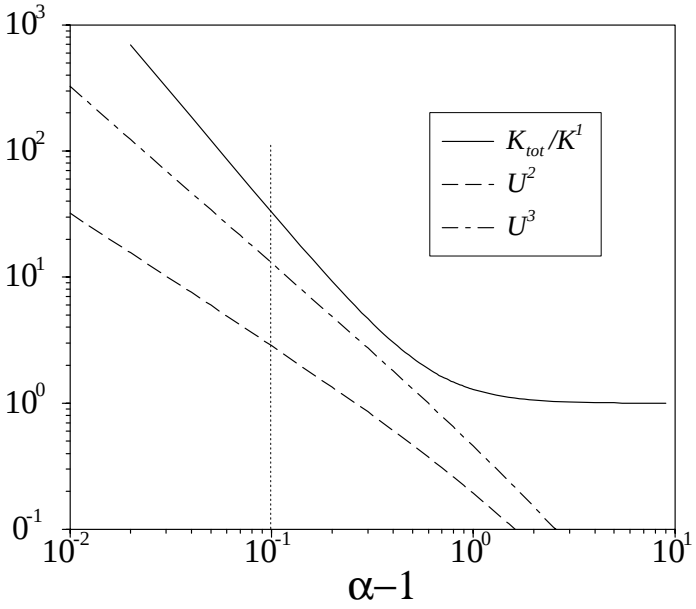

Figure 11: Total pressure drop normalized by that in duct 1 and average velocities in the subregions 2 and 3 as a function of the aspect ratio α. The total pressure drop increases rapidly when $\alpha \to 1$ and approaches the value as in duct 1 as $\alpha \gg 1$. TAURO is indicated by the dotted line.

value. This has its reason in the fact that the length of the subregion 2 measured between two Hartmann walls is half the one in subregion 3 taken at the position of the internal parallel layer at $z = -1$. For $-1 < z < 0$ the velocity profile $\bar{u}_c^2$ takes values proportional to $H - h$, the dimension of the cross section measured along the field lines. This is favorable for heat transfer reasons because the heat input to the fluid is higher near $z = -1$ than near $z = 0$. Similar results hold for duct 1, where the velocity profile as in insulating circular pipes is found, $\bar{u}_c^1 \sim h$.

It should be noticed that at $z = -1$ the core velocity jumps by a factor of two and may therefore cause different heat transfer properties at both sides of the internal parallel layer, where the heat input is almost the same. This may lead to large differences in temperature between both subregions and may cause thermal stresses within the structural material. The abrupt jump of velocity can be avoided easily by inserting a small piece of wall along the z axis between the outer and the inner walls, between the points $z = -\alpha$ and $z = -1$. By doing so the velocities $\bar{u}^3$ and $\bar{u}^2$ will be continuously connected as $z \to -1$.

Finally one should perform detailed heat transfer calculations to determine whether the relatively small velocity at $z = -\alpha$ is large enough to remove the heat introduced into the fluid near this point by surface heat flux and volumetric heating. Both contributions of heat input are largest at this position. A small gap size or an aspect ratio α near unity may help to keep the temperatures at acceptable values.

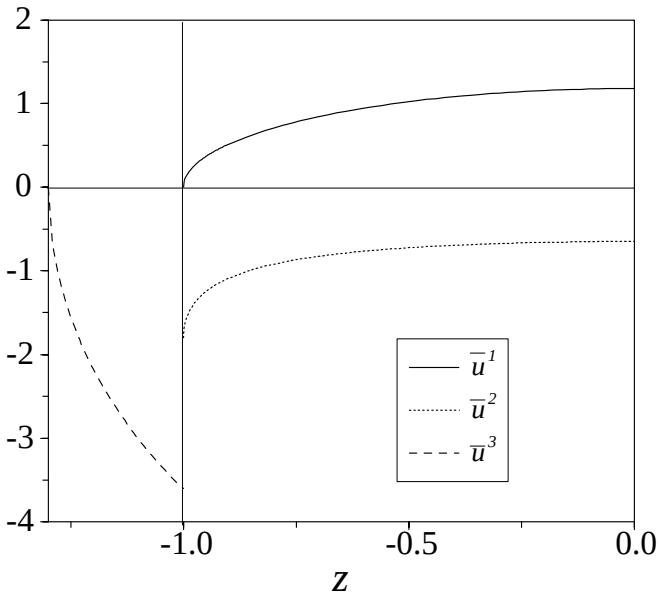

Figure 12: Average core velocities in duct 1 and in subregions 2 and 3.

5.2 Walls with high normal conductance

Another type of solution may be derived for the case of high normal conductance, when the $s \gg M^{-1}$.

The summation of equation (25) and (26) yields after integration

$$K^1 h + K^2 (H - h) + 3A = M^{-1} \partial_z \left(\bar{\phi}_c^1 + 2\bar{\phi}_c^2 \right), \tag{66}$$

where A has been introduced as integration constant. The summation of equations (27) and (26) leads to

$$4 \frac{\Delta \phi_c^2}{H - h} + 2K^2 H' = 0, \tag{67}$$

when the singular perturbation terms are neglected for the outer solution. For the same conditions one can evaluate the difference between the equations (27) and (26) and find

$$2\sqrt{1 + h'^2}\, s \left(\bar{\phi}_c^1 - \bar{\phi}_c^2 + \Delta \phi_c^2 \right) + 2K^2 (H' + h') = 0 \tag{68}$$

and further with equation (67)

$$\bar{\phi}_c^1 - \bar{\phi}_c^2 = -\frac{1}{\sqrt{1 + h'^2}\, s} K^2 (H' + h') + \frac{1}{2} K^2 H' (H - h). \tag{69}$$

There are now two equations (66) and (69) available for the determination of the two unknowns $\bar{\phi}_c^1$ and $\bar{\phi}_c^2$. Order of magnitude arguments show that as long as sM is large, equation (66) simplifies to

$$M^{-1} \partial_z \bar{\phi}_c^1 \approx M^{-1} \partial_z \bar{\phi}_c^2 = \frac{1}{3} \left[K^1 h + K^2 (H - h) \right] + A + O\left([sM]^{-1} \right) \tag{70}$$

a condition that is valid except in layers of thickness $\delta \sim \sqrt{sM}$ at the right or left side of the electrically coupled subregions, near $z = -1$ or $z = 0$.

Near $z = 0$ the potential requires some additional corrections due to the type of the equations which are singularly perturbed as $s \gg M^{-1}$. Using the stretched coordinate $\zeta = \sqrt{\frac{3}{2} sM}\; z$ (near $z = 0$ where $H' = h' = 0$) the equations for the potential corrections, denoted as $\hat{\phi}$, simplify to

$$\hat{\phi}_c^1 - \hat{\phi}_c^2 - \frac{3}{2} \partial_{\zeta\zeta} \hat{\phi}_c^1 = 0, \tag{71}$$

$$-\hat{\phi}_c^1 + \hat{\phi}_c^2 - 3 \partial_{\zeta\zeta} \hat{\phi}_c^2 = 0. \tag{72}$$

The stretching of the layer coordinates is motivated by the results obtained for the model geometry and leads to the most simple representation of the results. As in the case with the model geometry it is assumed that these layers are thicker than the usual MHD side layers, $\sqrt{\frac{3}{2} sM} \ll \sqrt{M}$.

The non-trivial solutions that vanish outside the layer become

$$\hat{\phi}_c^1 = -2\hat{B} \exp(\zeta), \quad \hat{\phi}_c^2 = \hat{B} \exp(\zeta). \tag{73}$$

The composite solutions for the potential gradients in both subregions become

$$M^{-1}\partial_z\bar{\phi}^1 = \frac{1}{3}\left[K^1 h + K^2\left(H-h\right)\right] + A - 2B\exp\left(\zeta\right), \tag{74}$$

$$M^{-1}\partial_z\bar{\phi}^2 = \frac{1}{3}\left[K^1 h + K^2\left(H-h\right)\right] + A + B\exp\left(\zeta\right), \tag{75}$$

where the integration constant B replaces the $\hat{B}$, introduced earlier. The unknown constants of integration A and B are determined by the fact that at the right side of the subregion 1 and at the right side of subregion 2 the integral current must vanish when the side walls are assumed to be insulating.

$$\begin{aligned} \int_0^h j_z^1 dy &= K^1 h - M^{-1}\partial_z\bar{\phi}_c^1 &&= 0 \quad \text{at} \quad z,\zeta = 0, \\ \int_h^H j_z^2 dy &= K^2\left(H-h\right) - 2M^{-1}\partial_z\bar{\phi}_c^2 &&= 0 \quad \text{at} \quad z,\zeta = 0. \end{aligned} \tag{76}$$

This leads to the result

$$A = 0, \quad B = \frac{1}{3}\left[\frac{1}{2}K^2\left(H-h\right) - K^1 h\right]. \tag{77}$$

It is expected that near $z=-1$ such layers of exponential type do not exist since even if the terms involving second order derivatives in equations (25,26) may become large, they may not be balanced by any of the other terms when $z \to -1$ because then $h' \to \infty$.

The result for subregion 3 remains unchanged as in the insulating case.

$$K^2 H = M^{-1}\partial_z\bar{\phi}_c^3. \tag{78}$$

In a further step one can combine the equation (17) determining the velocity with Ohm's law (11) and find $\bar{u} = \partial_z\bar{\phi}$ at leading order of approximation for each subregion, using the solutions for potential derived just above. The corresponding flow rates are obtained by integration over the sub-regions.

$$q^1 = \int_{-1}^{0} h\,\bar{u}^1\,dz, \tag{79}$$

$$q^2 = \int_{-1}^{0} \left(H-h\right)\,\bar{u}^2\,dz, \tag{80}$$

$$q^3 = \int_{-\alpha}^{-1} H\,\bar{u}^3\,dz. \tag{81}$$

The normalization of the velocity in duct 1, $q^1 = \pi/4$ and the integral flux balance $q^1 + q^2 + q^3 = 0$ gives two equations for the two unknown pressure gradients K^1 and K^2. The lengthy expressions are omitted here.

Instead the results for the total pressure drop $K_{tot} = K^1 + |K^2|$ normalized by the pressure drop in an insulating central duct 1 is plotted in figure 13. The pressure drop exhibits a similar behavior as for insulating conditions namely a strong increase when $\alpha \to 1$ (high pressure drop in the gap) and approaches a finite value as $\alpha \gg 1$. However, even for high values of the product sM the pressure drop does not increase by orders

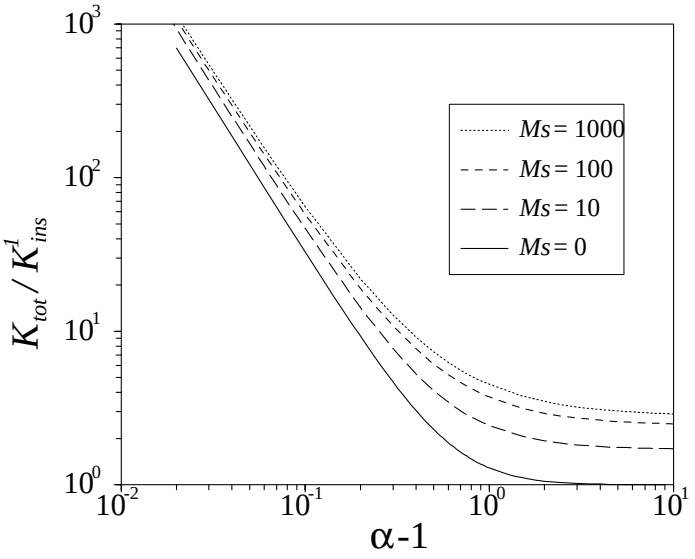

Figure 13: Total pressure drop scaled with that in an insulating duct 1 as a function of the aspect ratio α for different values of the wall normal conductivity. For comparison the curve for perfectly insulating walls is included

of magnitude. This will become more clear when considering the dependence on this quantity in figure 14. The result of these considerations is comparable to that derived for the model geometry where the pressure drop is increased with the product sM but only up to a certain factor. This factor is of course dependent on the aspect ratio α and is smaller than one order of magnitude for the cases considered in figure 14. For better insulation, i.e. smaller sM values the pressure drop is decreased. Unfortunately the analysis performed is valid for $\sqrt{sM} \gg 1$ only, so that it is not possible to continue the solution towards insulating conditions as $sM \to 0$. Nevertheless results for insulating ducts are known from the previous subsection and indicated within the figure as filled symbols to get an overall consistent picture.

From the results derived above for the TAURO geometry one could draw the conclusion that there is an influence from non perfect wall-normal insulation, but with only little consequences on the overall performance (besides a higher pressure drop). This however is not the case because the flow pattern in the duct 1 and in subregion 2 is significantly changed. While TAURO has been designed to have a downward flow in subregion 2 and an upward flow in duct 1 one finds now for $sM = 1000$ a strong coupling of the flow in both regions (see figure 15). Near $z = -1$ the influence of subregion 2 wins because the extension of this domain along the magnetic field lines is much larger than that of duct 1. The flow in region 2 is pulling that in duct 1. For $z \to 0$ except within the layers near $z = 0$ the flow in duct 1 wins over that in subregion 2 and carries the latter one in its own flow direction upwards. Near $z = 0$ one observes exponential layers of typical thickness $\left(\frac{3}{2}sM\right)^{-1/2}$. Within the layer the coupling between the subregions develops to the almost perfect coupling as $\sqrt{\frac{3}{2}sM}\,|z| \gg 1$. The weakest coupling is close

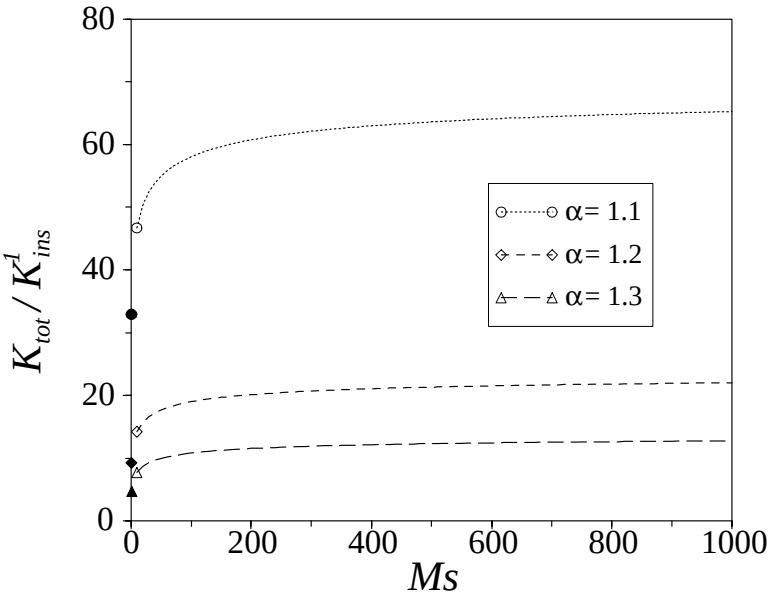

Figure 14: Total pressure drop as a function of the insulation quality

to $z = 0$, where the flow follows the applied pressure gradients.

From the viewpoint of heat transfer such flow pattern may be undesirable because there will develop closed recirculation loops in subregion 2 involving part of subregion 3. One smaller loop exists neat $z = 0$ where the downward jet balances part of the upward flow in the core. The other loop involves the core 2 where more fluid flows upwards than downwards near $z = -1$. The rest of the upward flow from subregion 2 has to be balanced by an increased downward flow in subregion 3. Closed loops will not contribute significantly to heat transfer and should be excluded in the application.

For lower values of sM the exponential layers become thicker, the peak values near $z = 0$ reduce and both regions 1 and 2 decuple gradually as $sM \to 0$ to exhibit the profiles as already shown in figure 12, where the flow direction is as desired. Decupling requires $\sqrt{sM} \ll 1$ the condition that guaranties perfect insulation.

Returning to the dimensional quantities $\sigma_w \ll \sigma \frac{t}{a} M^{-1} \approx 2.6 \frac{1}{\Omega m}$ or equivalently a resistivity of $0.38 \Omega m$ is required to obtain the designed flow directions. This condition is hardly to be achieved using the data specified during the introduction where $\sigma_w = 2 - 10^2 \frac{1}{\Omega m}$ (http://www.mortoncvd.com/sicprop1.htm). With such data the coupling will not be as strong as shown in figure 15 but the subregions are by far not decoupled. There is a hope that the SiC/SiC composite material may have reduced conductivity. One order of magnitude would be good, one more desirable. In any case it may be favorable to have some safety margin since the effect of irradiation damage on the conductivity is unclear at present day.

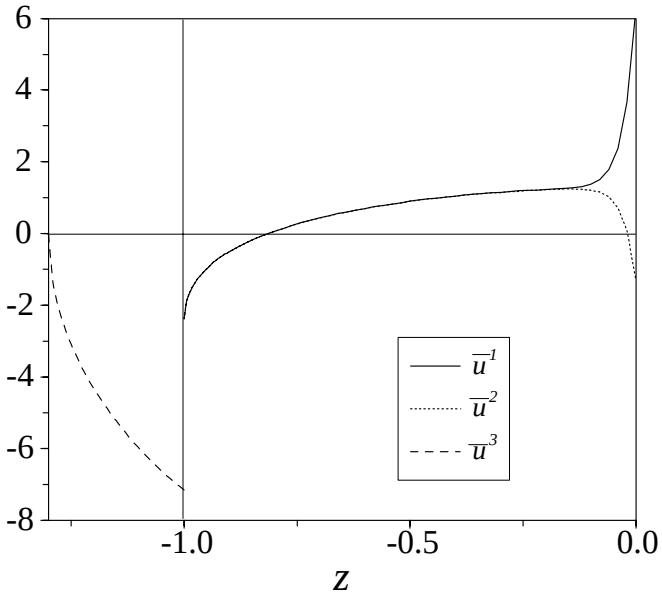

Figure 15: Average core velocity profile in duct 1and subregions 2 and 3. The flows in subregion 2 and duct 1 are strongly coupled.

6 Improvements of the TAURO MHD performance

The results that have been outlined during the previous section showed that there might be a problem of heat transfer in the present TAURO blanket design because closed recirculation loops appear in the first wall coolant annular duct. With the present day knowledge about the wall electric conductivity one can not definitively exclude that undesired flow pattern. In the following some suggestions for an improved design are discussed.

The most simple proposal is that of using a wall material with better insulating properties than that used in the calculations above. This may be difficult from a first point of view because the requirement of high thermal conductivity at the first wall may lead to wall material with increased electrical conductivity. On a closer view, however, one will discover that high thermal conductance is required only near the first wall. The common wall which is separating the flow between subregion 2 and duct 1 does not need such values. It is especially this wall that dominates the MHD flow in the present design. One proposal for an improvement may be to use the wall material with high thermal conductance at the first wall only and to use standard 2D woven material at the dividing wall. The fibers that are oriented in the wall tangential direction may increase the wall tangential conductance by some amount, but there is some chance to have still high insulation normal to the wall, where it is mostly required. Detailed material testing is recommended to check if under such assumptions the values of electrical resistivity can be achieved as they are required.

A second proposal from a theoretical point of view may be to change slightly the design and to use a double wall separating the duct 1 and subregion 2. The double wall can be produced by any SiC composite material but it should ensure a small gap (no liquid metal inside) to avoid currents crossing the wall from one subregion to the other. For availability reasons it may be difficult to maintain a liquid metal free gap for a longer period of operation so that such an improvement seem to be academic.

The most promising improvement on the basis of the present day SiC material requires some changes of the design. The overall shape of a poloidal cross section will remain unchanged, but the feeders and bends at the top and bottom of the blanket require some modification. It is proposed to change the flow direction in the duct 1. If the flow in duct 1 has the same direction as the flow in the annular gap all negative effects concerning the flow direction as discussed above do not occur or are small even for high wall normal conductance. Moreover, a flow coupling will have positive implications on the overall performance. One could think about the possibility to use the duct 1 to drive electrically the flow in the annular gap or vise versa. Possible velocity profiles are shown in figure 16. It has been assumed in this example that the flow rates in the annular gap and in duct 1 are equal, $q^1 = q^2 + q^3$. The results are shown for an aspect ratio $\alpha = 1.3$ and for high wall normal conductance $sM = 1000$. The flow in subregion 2 is strongly coupled to that in duct 1 and the exponential layers near $z = 0$ are still present. Nevertheless, recirculation loops do not occur for the values of parameters as considered here. The coupling of the flows leads to almost uniform core velocity distribution along z. The velocity profile in region 3 remains qualitatively. It is strongly increasing with increasing z.

A forced flow in duct 1 with similar flow rate as in the annular gap resolves the

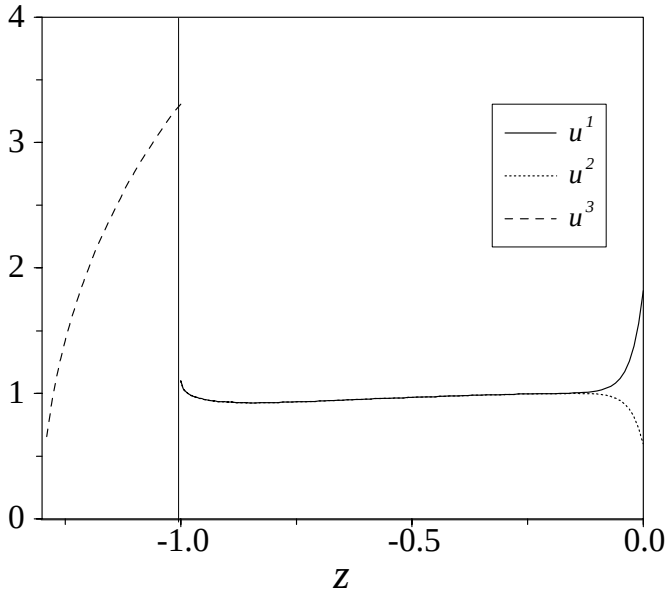

Figure 16: Core velocity profile in duct 1 and subregions 2 and 3. The flows in subregion 2 and duct 1 are strongly coupled. The aspect ratio is $\alpha = 1.3$ and $Ms = 1000$.

problem of flow reversal in the annular gap but reduces the final heat up of the liquid metal and leads to lower exit temperatures because the total flow rate would be doubled. To overcome this problem one could think about the possibility to drive the flow in duct 1 by the electrical coupling with the annular gap and to give the flow the possibility to exchange with one of the rear channels, which are not yet considered in the present analysis. By doing so it should be possible to reach similar values for heat up as originally planned. This point could be the subject of further investigation.

Besides the desirable results for poloidally fully developed flow as shown in figure 16 there are other arguments for choosing such flow directions. In the original design where the annular gap flow is opposite to the flow in duct 1 it is necessary to turn the flow at the bottom of the blanket from the gap towards the center duct 1. It is not a big MHD issue to turn the flow from subregion 3 to duct 1 because such turns are performed mainly in a plane perpendicular to the magnetic field and require therefore only little pressure drop (see e.g. Molokov (1994)). This is, however, not the case when the turn from subregion 2 to duct 1 is considered. Bend flows in a plane containing magnetic field lines are undesirable because they cause highest MHD pressure drop and strong 3D deformations of the velocity profiles (compare Molokov and Bühler (1994)). It is to be expected that the flow in subregion 2 turns both, towards $z = 0$ and/or towards subregion 3 before it will reach the bending position. The reason is an unavoidable electrical short cut at the bottom of the blanket, at the bend, where ducts with opposite electrical potential are coupled via the liquid metal. Even perfect electrical insulation of the walls would not help in this case and one has to expect regions with very small velocities or recirculation loops near the blanket bottom. If the flow direction in duct 1 and the annular gap are equal this problem is not present. At the bottom one could collect the flow and turn it

(in a plane perpendicular to the magnetic field) towards the rear rectangular poloidal channels.

Flow coupling between the rear poloidal channels is present as well. The coupling there has no negative effects because the pressure drops and flow directions are equal when considered along a field line. If there would be any difference in pressure drop, the coupling established equal flow rates and homogenized the heat transfer among the channels along the toroidal direction. Thus, coupling in the rear poloidal channel is favorable for the MHD performance of the whole blanket.

References

Bühler, L. and Molokov, S.: 1993, Magnetohydrodynamic flows in ducts with insulating coatings, *Technical Report KfK 5103*, Kernforschungszentrum Karlsruhe.

Bühler, L. and Molokov, S.: 1994, Magnetohydrodynamic flows in ducts with insulating coatings, *Magnetohydrodynamics* **30**(4), 439–447.

Chang, C. and Lundgren, S.: 1961, Duct flow in magnetohydrodynamics, *ZAMP* **XII**, 100–114.

Giancarli, L., Bonal, J. P., Caso, A., Marois, G. L., Morley, N. B. and Salavy, J. F.: 1998, Design requirement for SiC/SiC composites structural material in fusion power reactor blankets, *Fusion Engineering and Design* **41**, 165–171.

Gold, R. R.: 1962, Magnetohydrodynamic pipe flow. Part 1, *Journal of Fluid Mechanics* **13**, 505–512. compare Shercliff.

Hunt, J. C. R.: 1965, Magnetohydrodynamic flow in rectangular ducts, *Journal of Fluid Mechanics* **21**, 577–590.

Hunt, J. C. R. and Stewartson, K.: 1965, Magnetohydrodynamic flow in rectangular ducts, *Journal of Fluid Mechanics* **23**, 563–581.

Kumamaru, H.: 1984, Magnetic pressure drop and heat transfer of liquid metal flow in annular channel under transverse magnetic field, *Journal of Nuclear Science and Technology* **21**(5), 393–400.

Malang, S. and Tillack, M. S.: 1995, Development of self-cooled liquid metal breeder blankets, *Technical Report FZKA 5581*, Forschungszentrum Karlsruhe.

Miyazaki, K., Gonno, Y., Nakano, M., Konishi, K., Inoue, S. and Yamaoka, N.: 1988, MHD pressure drop of NaK flow in a coaxial double circular duct and a plane-insulated duct under transverse magnetic field, *Proceedings of the Fourth International Conference on Liquid Metal Engineering and Technology, Avignon, 17-21 Oct*, pp. 437/1–10.

Molokov, S.: 1993, Fully developed liquid-metal flow in multiple rectangular ducts in a strong uniform magnetic field, *European Journal of Mechanics, B/Fluids* **12**(6), 769–787.

Molokov, S.: 1994, Liquid metal flows in manifolds and expansions of insulating rectangular ducts in the plane perpendicular to a strong magnetic field, *Technical Report KfK 5272*, Kernforschungszentrum Karlsruhe.

Molokov, S. and Bühler, L.: 1994, Liquid metal flow in a U-bend in a strong uniform magnetic field, *Journal of Fluid Mechanics* **267**, 325–352.

Moreau, R.: 1990, *Magnetohydrodynamics*, Kluwer Academic Publisher.

Pérez, A. S., Giancarli, L., Molon, S. and Salavy, J. F.: 1995, Progress on the design of the TAURO breeding blanket concept, *Technical Report DMT 95/575 (SERMA/LCA/1829)*, CEA.

Tillack, M. S., Wang, X. R., Pulsifer, J., Malang, S., Sze, D. K., Billone, M. and Sviatoslavsky, I.: 1999, Fusion power core engineering for the ARIES-ST power plant, *Fusion Engineering and Design* p. to be published.